Journal of Membrane Science 718 (2025) 123636

Contents lists available at ScienceDirect

Journal of Membrane Science

journal homepage: www.elsevier.com/locate/memsci

Counter-ion mobility in cation-exchange membranes: Single electrolytes versus mixtures

Alaaeldin A.E. Elozeiri [a], Rob G.H. Lammertink [b], Shihong Lin [c], Huub H.M. Rijnaarts [a], Jouke E. Dykstra [a,*]

[a] Environmental Technology, Wageningen University & Research, Bornse Weilanden 9, 6708 WG, Wageningen, Netherlands
[b] Membrane Science and Technology, Faculty of Science and Technology (TNW), University of Twente, Drienerlolaan 5, 7522 NB, Enschede, Netherlands
[c] Department of Civil and Environmental Engineering, Vanderbilt University, Nashville, TN, 37235, USA

ARTICLE INFO

Keywords:
Diffusion coefficient
Ion mobility
Selectivity
Electrodialysis
Ion-exchange membrane

ABSTRACT

Many electrochemical technologies utilize ion-exchange membranes for water treatment (e.g. electrodialysis), energy conversion applications (e.g. redox flow batteries), and electrochemical synthesis (e.g. bipolar membrane electrodialysis). Ion mobility inside the membrane plays a primary role in determining the energy efficiency and ion selectivity of the process. We investigated the mobility of Na^+, K^+, Mg^{2+}, and Ca^{2+} inside commercial cation-exchange membranes based on conductivity measurements in single electrolyte solutions. Moreover, we employed a transport model to simulate two scenarios for the counter-ion mobilities in a binary mixture of Na^+ and Mg^{2+}. In a single electrolyte, the mobility of various counter-ions is reduced to different extents mainly based on the membrane water volume fraction as well as the ion hydration. For example, in membranes with low-to-moderate water volume fractions, the Mg^{2+} mobility is 9–17 times more reduced than the mobility of Na^+. In a mixture, this difference in mobility reduction is less pronounced since the ions are limited by the surrounding counter-ions inside the membranes. In this regard, the counter-ion mobilities for a single electrolyte do not necessarily reflect the counter-ion selectivity during multi-electrolyte experiments. Furthermore, the counter-ion selectivity in electrodialysis is highly influenced by the ion partitioning within the membrane in addition to ion mobilities in the diffusion boundary layer.

1. Introduction

Electrochemical technologies [1,2] are promising for fit-to-purpose water treatment processes [3,4] as well as the recovery of valuable ions, e.g., NH_4^+ [5], Li^+ [6], and La^{3+} [7]. Low energy consumption is a key indicator of a sustainable treatment process [8]. Moreover, a high flux selectivity is desirable for the separation or purification of an ionic species from a multi-ionic solution [9]. Several electrochemical technologies, e.g., electrodialysis and fuel cells, rely on ion-exchange membranes as selective separators [10]. In electrodialysis, both aspects, i.e., energy consumption and ion selectivity, are tightly connected to the counter-ion mobility inside the membrane [11].

The presence of some ions in raw or wastewater streams can ruin the energy efficiency of the electrochemical process. Multivalent cations, e.g., Mg^{2+} and Ca^{2+}, deteriorate the performance of fuel cells [12–14], reverse-electrodialysis [15–18], microbial reverse-electrodialysis cells [19], and electrodialysis [20]. This can be explained by the low conductivity of the multivalent ions in most of the ion-exchange membranes. For example, the conductivity of cation-exchange membranes (CEMs) with Mg^{2+} as the counter-ion can be one order of magnitude lower than a membrane with Na^+ counter-ions [21,22].

The membrane tortuosity can explain the reduced mobility of monovalent ions of a relatively small hydrated radius, such as Na^+, inside ion-exchange membranes [23,24]. The mobilities of different ionic species can vary tremendously inside the same membrane relative to the ion mobility in aqueous solutions. Fan et al. [25] used two (membrane-specific) fitting parameters to capture the effects of membrane tortuosity and electrostatic interactions on the counter-ion mobility in single salt experiments. They suggested a relation between the counter-ion diffusion coefficient inside the membrane (D_i^m) relative to the diffusion coefficient in aqueous solutions (D_i^{aq}) and its valency squared (z_i^2)

* Corresponding author.
E-mail address: jouke.dykstra@wur.nl (J.E. Dykstra).

https://doi.org/10.1016/j.memsci.2024.123636
Received 11 October 2024; Received in revised form 16 December 2024; Accepted 18 December 2024
Available online 20 December 2024

$$\ln \frac{D_i^m}{D_i^{aq}} \propto -A \cdot z_i^2 \quad \text{Eq. 1}$$

where the proportionality constant, A, is a membrane-specific parameter [25]. However, the mobility of counter-ions inside the membrane can be reduced by different factors even if they carry the same charge [26]. For example, the diffusion coefficient of Li^+ inside the membrane is further reduced than that of Na^+ followed by K^+ and Cs^+ [26–29], which is not explained by the membrane tortuosity [26] nor by the ion valency proposition (Eq. 1).

Another theoretical framework is the counter-ion condensation theory which assumes a fraction of counter-ions to be immobilized, or "condensed" [30]. This assumption led to significant underestimations of the membrane conductivity in case of monovalent counter-ions (Fig. 2 in Ref. [31]). Extending the framework to consider two mobile categories of counter-ions (instead of a mobile and an immobile fraction) led to better estimations of the membrane conductivity in case of monovalent counter-ions but the framework significantly overestimated the conductivity for multivalent counter-ions (Fig. 3 in Ref. [31]).

The counter-ion mobility can be calculated based on the membrane conductivity in a single electrolyte solution, e.g., NaCl, $MgCl_2$, or Na_2SO_4 [21–23]. The partitioning of the different ionic species inside the membrane can be estimated based on membrane equilibrium experiments in mixtures [22]. The counter-ion fluxes in mixtures depend on the ion partitioning and mobility inside the membrane. However, discrepancies arise between the experimental fluxes in mixtures and the theoretical predictions that assign the counter-ion diffusion coefficients to the values measured in single electrolyte experiments [22]. Furthermore, the ratio between the counter-ion mobilities or membrane conductivities during single electrolyte experiments does not reflect the actual flux selectivity for the two counter-ions during an electrodialysis experiment of a mixture of those ionic species [7,21,32].

Tracer diffusion experiments [33,34] provide further insights into the dependency of ion mobility on the other ionic species present in the membrane. Forssell [35] measured the Na^+ self-diffusion coefficient in a CEM as $1.1*10^{-10}$ m^2/s. Furthermore, the Na^+ tracer diffusion coefficient ($D^{TR}_{Na^+}$) varied in the range of $[0.1–1.5]*10^{-10}$ m^2/s depending on the counter-ion species present in the membrane where $D^{TR}_{Na^+}$ increased in the sequence of $Mg^{2+} < Li^+ < Na^+ < K^+$. The effect of the abundantly present ionic species on the Na^+ diffusion is much more pronounced in the membrane compared to its effect in aqueous solution. In this regard, the transport of the Na^+ traces inside the membrane is assumed to be mainly governed by exchanging positions with the surrounding counter-ions.

In this study, we dissect the major factors controlling the ion mobility inside ion exchange membranes. We specifically explore the impact of the membrane reinforcement structure, water volume fraction, and counter-ion properties on the membrane conductivity. Moreover, we compare two scenarios for describing the counter-ion mobility during electrodialysis of a binary mixture: (1) using an independent diffusion coefficient for each species versus (2) using an averaged diffusion coefficient for both counter-ions. Finally, we compare the transport selectivity based on each scenario to the experimental values.

2. Materials & methods

Seven commercial ion-exchange membranes were investigated: Fujifilm CEM type-10 and type-12 (Fujifilm Manufacturing Europe BV, The Netherlands), Selemion CMTE and CMVN (Asahi Glass Co., Japan), and Fumasep FKS-PET-130, FKB-PK-130, and FKD-PK-75 (Fumatech BWT GmbH, Germany). Solutions were prepared using Milli-Q water (Millipore) and the salt of interest. Reagent-grade salts were purchased from Sigma-Aldrich (Na_2SO_4, KCl, K_2SO_4, $MgSO_4$, $MgCl_2$, and $CaCl_2$) and VWR Chemicals (NaCl). All experiments were performed at 19–22 °C unless otherwise stated.

Common membrane characteristics, e.g., wet thickness, water content, and ion-exchange capacity are reported in Ref. [23] and in the Supporting Information, SI-2. The ion activity coefficients inside the membranes are retrieved from Ref. [22]. The reinforcement structure was observed via phase-contrast Nikon Eclipse E400 microscope under 10–40x magnification for dried membrane samples.

2.1. Electrochemical characterization

We characterized the electrochemical behavior of the coated and bare membranes via linear potential sweep (direct current, DC) and electrochemical impendence spectroscopy (EIS) using a 6-compartment electrodialysis cell (6C-ED). Measurement details and resistance calculations are explained in Ref. [23]. The membrane samples were equilibrated in the solution of interest, where the solution was refreshed three times. We characterized the membrane samples in single electrolyte solutions of 0.5 M NaCl and KCl as well as 0.25 M Na_2SO_4, K_2SO_4, $MgSO_4$, $MgCl_2$, and $CaCl_2$. Moreover, we measured the membrane resistance in a binary mixture of 0.25 M NaCl +0.125 M $MgCl_2$ where the Na^+:Mg^{2+} molar ratio is 2:1 (i.e., the Na^+:Mg^{2+} equivalent molar ratio is 1:1). For all the investigated solutions, the total concentration of the cationic charges is 0.5 M. All measurements were repeated twice. The membrane resistance is the difference between the combined (membrane + solution) resistance and the blank (solution only) resistance. For Na^+ and K^+ solutions, an area reducer was used so that the membrane resistance is significant relative to the blank resistance (Eq. 19 in Ref. [23]). The solutions were circulated through the 6C-ED at 0.27 ± 0.02 L/min and 20 ± 0.2 °C.

2.2. Influence of the membrane reinforcement

To improve their mechanical strength, commercial IEMs are usually backed with a reinforcement material [36–39]. The membranes of CMTE, FKS, FKD, and FKB are reinforced with a woven monofilament mesh (Fig. 1a). The reinforcement of Fuji-CEM-10 and 12 has the structure of a nonwoven fabric. For CMVN, the reinforcement structure resembles a porous layer that embeds the ion-exchange resin within its connected gaps on the micrometer scale.

The overall resistivity (ρ_m [Ω.m]) and conductivity (κ_m [S/m]) of the composite membrane can be calculated as follows [11]

$$\rho_m = \frac{R_m}{\delta_m} \quad \text{Eq. 2}$$

$$\kappa_m = \frac{1}{\rho_m} \quad \text{Eq. 3}$$

where R_m [$\Omega.m^2$] is the membrane-area resistance and δ_m [m] is the wet membrane thickness. Ions cannot access the volume occupied by the reinforcement material of the membrane. Therefore, expressing the membrane parameters on the basis of the active swollen polymer volume (i.e., excluding the volume of the reinforcement material) leads to a more accurate analysis of the ion transport. For the membranes reinforced with a woven mesh, we corrected the membrane parameters to represent the effective values in the swollen polymer volume. For the non-woven reinforcement, the correction for the reinforcement volume is intricate, and therefore the parameters of CMVN, Fuji-CEM-10, and 12 are not corrected. The ionic charge density within the membrane resin or active volume (ICD^{rs} [mol/m^3 swollen polymer]) is calculated as follows [23].

$$ICD^{rs} = \frac{ICD}{1 - f_X^{vol}} \quad \text{Eq. 4}$$

where ICD [mol/m^3 wet IEM] is the ionic charge density of the membrane on the basis of the total wet membrane volume (Table SI-4). The superscript "rs" refers to the ion-exchange resin phase inside the

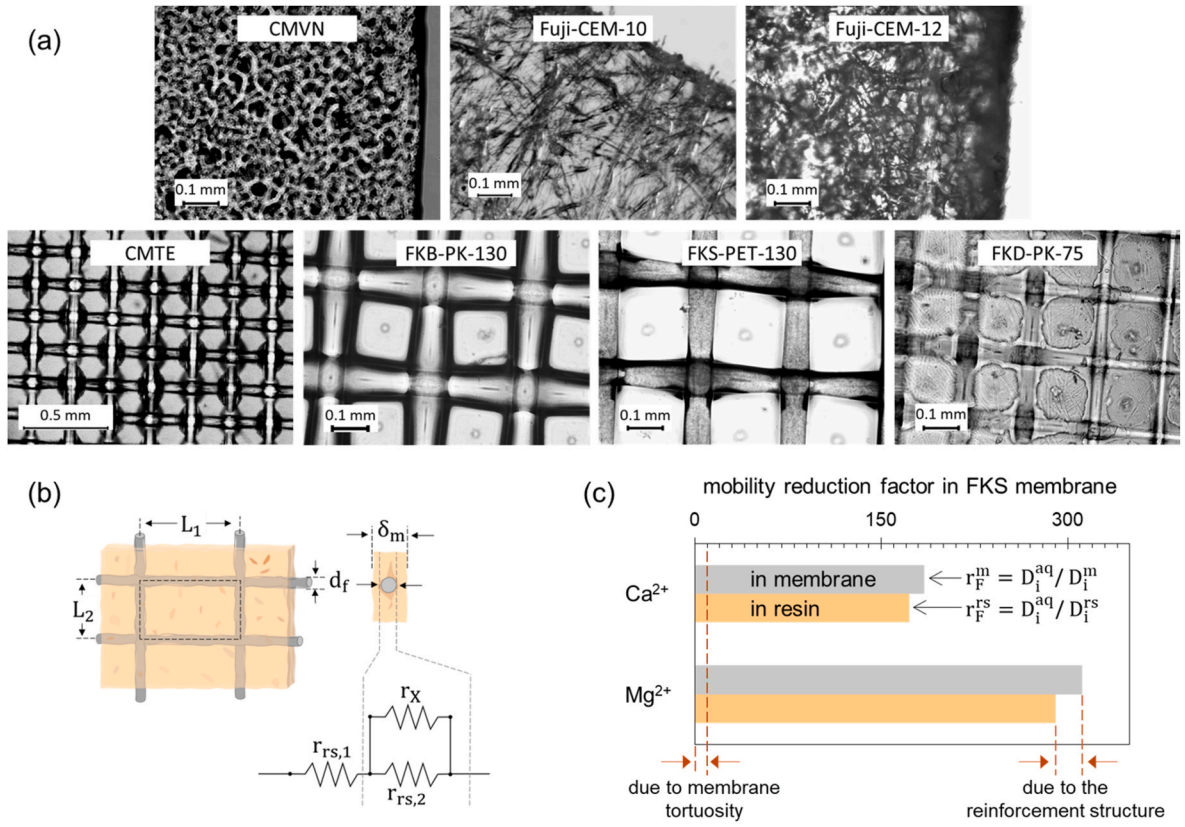

Fig. 1. (a) Optical micrographs of reinforced ion-exchange membranes. (b) The structure of an IEM supported by a woven reinforcement with filament diameter d_f. The repeating unit is marked by a dashed rectangle with dimensions L_1 and L_2. The equivalent circuit of a composite IEM at the ohmic regime where $r_{rs,1}$ and $r_{rs,2}$ are the resistances of the resin and r_X is the reinforcement resistance. (c) The mobility reduction factor in FKS membrane based on the measured EIS resistance at 0.25 M $CaCl_2$ and $MgCl_2$. The grey bars represent the reduction factor in the whole membrane while the light orange bars represent the reduction factor in the membrane resin. The reduction factor due to the membrane tortuosity is estimated based on the Mackie and Meares theory and the membrane water volume fraction. (For interpretation of the references to colour in this figure legend, the reader is referred to the Web version of this article.)

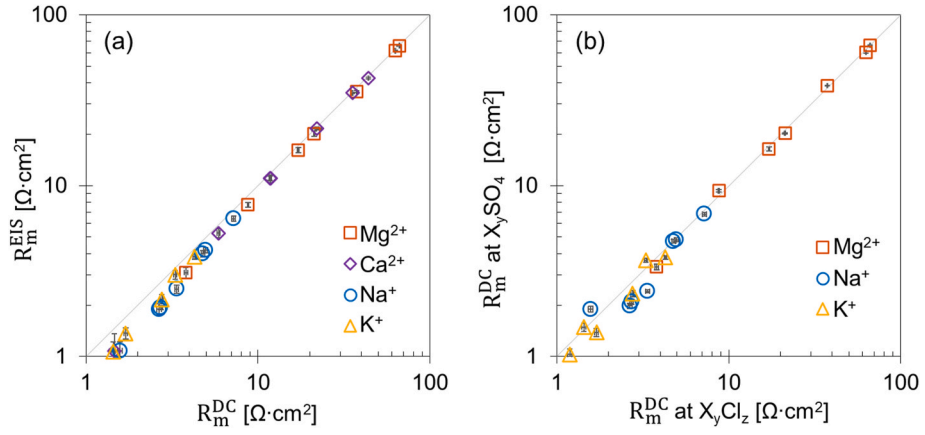

Fig. 2. (a) Membrane-area resistance measured via electrochemical impendence spectroscopy versus direct current at 0.25 M $MgCl_2$, 0.25 M $CaCl_2$, 0.5 M NaCl, and 0.5 M KCl. (b) Membrane-area resistance in sulfate electrolytes versus the corresponding chloride electrolytes, e.g., 0.25 M Na_2SO_4 versus 0.5 M NaCl. The EIS resistance is determined based on the real impedances in the frequency range of 1–500 Hz. The DC resistance is calculated via linear fitting of the current-voltage data. The error bars represent the uncertainty in the resistance measurements and the membrane active area. For EIS resistance, the uncertainty represents the standard deviation of the data. For DC resistance, the uncertainty is calculated based on the standard error and a confidence level of 0.9. Further details are given in Ref. [23].

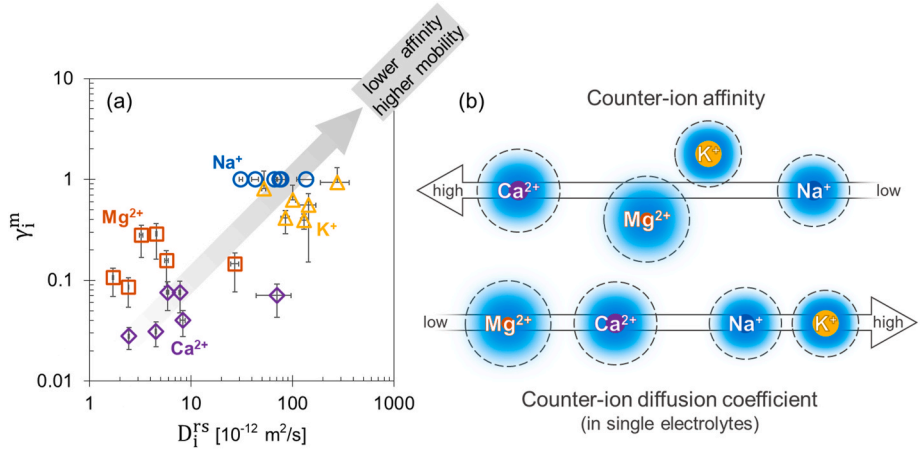

Fig. 3. (a) Ion diffusion coefficients inside the membrane resin (x-axis) versus ion activity coefficients (y-axis) for different cation-exchange membranes. A higher activity coefficient translates to a lower affinity. The activity coefficient values are retrieved from Ref. [22]. The diffusion coefficients are calculated using the measured resistances via the direct current (DC) method. (b) A general trend of the counter-ion diffusion coefficient in single electrolytes (bottom) and the counter-ion affinity (top) in cation-exchange membranes.

membrane. The volume fraction of the reinforcement material (f_X^{vol}) is calculated as the ratio between the volume of the reinforcement material to the total volume of the wet IEM

$$f_X^{vol} = \frac{\pi \cdot d_f^{\,2} \cdot (L_1 + L_2)}{4 \cdot \delta_m \cdot L_1 \cdot L_2} \quad \text{Eq. 5}$$

where d_f [m] is the filament diameter of the reinforcement mesh (Table SI-3). The reinforcement mesh has a repeating unit with dimensions L_1 [m] and L_2 [m] (Fig. 1b).

In the ohmic regime [40], the IEM behaves as a resistor (Fig. 1b). The resistance due to the reinforcement material (r_X) is assumed to be high compared to the swollen polymer resin, i.e., $r_X \gg r_{rs,2}$. Therefore, the membrane resistance, r_m [Ω], of a repeating unit with dimensions L_1 and L_2 is expressed by two resistances in series as follows

$$r_m = r_{rs,1} + r_{rs,2} \quad \text{Eq. 6}$$

$$r_m = \frac{R_m}{A_u} \quad \text{Eq. 7}$$

where R_m [Ω.m^2] is the membrane-area resistance, and A_u is the repeating unit area ($A_u = L_1 \bullet L_2$). As discussed in the Supporting Information (SI-2), the membrane resin resistivity, ρ_m^{rs} [Ω.m], can be formulated as follows

$$\rho_m^{rs} \simeq \frac{R_m \cdot \left(1 - f_{X_1}^{area}\right)}{\delta_m \cdot \left(1 - f_{X_1}^{area}\right) + d_f \cdot f_{X_1}^{area}} \quad \text{Eq. 8}$$

where $f_{X_1}^{area}$ is the area fraction blocked by the reinforcement material. Moreover, the resin conductivity, κ_m^{rs} [S/m], is given by [41]

$$\kappa_m^{rs} = \frac{1}{\rho_m^{rs}} = \frac{F^2}{RT} \sum_i z_i^2 \cdot D_i^{rs} \cdot C_i^{rs} \quad \text{Eq. 9}$$

where z is the ion charge, D [m^2/s] is the diffusion coefficient, C [mol/m^3] is the concentration, R [J/(K·mol)] is the universal gas constant, F [C/mol] is Faraday's constant, and T [K] is the temperature. The subscript "i" refers to any mobile ion in the membrane. Relative to the aqueous solution, the ion mobility inside the membrane resin is reduced by a factor, $r_{F,i}^{rs}$, which is expressed as follows

$$r_{F,i}^{rs} = \frac{D_i^{aq}}{D_i^{rs}} \quad \text{Eq. 10}$$

where D_i^{aq} is the ion diffusion coefficient at infinite dilution (Table SI-1). We calculate the mobility reduction factor for each ion based on the membrane conductivity in a single electrolyte (SE) solution via Eqs. 8–10. The concentrations of counter and co-ions in the membrane are calculated using the ideal Donnan equilibrium condition and the electroneutrality principle [11,23,42]

$$\left(\frac{C_{ct}^m}{C_{ct}}\right)^{1/z_{ct}} = \left(\frac{C_{co}^m}{C_{co}}\right)^{1/z_{co}} \quad \text{Eq. 11}$$

$$z_{fix} \cdot C_{fix}^m + \sum_i z_i \cdot C_i^m = 0 \quad \text{Eq. 12}$$

where subscripts "ct", "co", and "fix", refer to the counter-ions, co-ions, and fixed-charged groups in the membrane, respectively. The concentration of fixed-charged groups is taken as the resin ionic charge density ([mol/m^3 swollen polymer], Eq. 4) and their charge (z_{fix}) is −1 for CEMs.

The water volume fraction of the membrane resin, $V_{H_2O}^{rs}$ [mL H_2O/mL swollen polymer], is calculated as follows

$$V_{H_2O}^{rs} = \frac{WC \cdot a_m}{\Gamma_w \cdot \delta_m \cdot \left(1 - f_X^{vol}\right)} \quad \text{Eq. 13}$$

where WC [g H_2O/g dry polymer] is the water content, a_m [g dry polymer/m^2 wet IEM] is the surface area density of membrane material, δ_m [m] is the membrane wet thickness, and Γ_w [g/mL] is the water density.

3. Results & discussion

3.1. Counter-ion mobility at single electrolytes

The membrane resistance can be measured via direct current (DC) or electrochemical impedance spectroscopy (EIS). The membrane resistance is the difference between the combined (membrane + solution) resistance and the blank (solution only) resistance. For the blank measurements, both methods measure the same solution resistance (the relative difference is ca. 1 %, Table SI-5). The membrane resistance measured via EIS is slightly lower than the DC method in the case of the monovalent counter-ion, i.e., Na^+ and K^+ (Fig. 2a). It is hypothesized that ions endure additional resistance under DC compared to alternating current due to the interfacial and diffusion boundary layer resistances as well as the ion-membrane friction [23,43]. In the DC measurement, the

ions move across the membrane in response to an applied potential. In the EIS measurement, the ions oscillate according to the signal frequency and amplitude. The difference between the DC and EIS resistance measurements is negligible in the case of multivalent counter-ions, inferring that the bulk resistance of the membrane is dominant over the interfacial resistance. We measured the membrane resistance for different chloride and sulfate salts (Fig. 2b). The type of co-ions, i.e., Cl^- or SO_4^{2-}, has a minor role in the measured membrane resistance in the experiments with Na^+ and K^+ counter-ions. In case of Mg^{2+} counter-ions, the co-ion type does not influence the membrane resistance. Similar results are reported in literature [31,44,45].

Ion transport inside IEMs is determined by the ion mobility and affinity (or partitioning). The counter-ion mobility and affinity are affected by common factors including membrane properties (e.g., membrane water content) and ion properties (e.g., ion charge and hydrated radius) [46]. Based on the Donnan equilibrium condition, cations of higher affinity inside a CEM have lower membrane activity coefficients (Eqs. 6, 34 and SI-9 in Ref. [22]). Generally, Na^+ and K^+ have lower affinity and higher mobility than Ca^{2+} and Mg^{2+} (Fig. 3). Counter-ions of equal valency can have higher affinity and mobility relative to another ion in the membrane as generally exhibited by K^+ relative to Na^+, and Ca^{2+} relative to Mg^{2+}. Therefore, the ion mobility is not exclusively limited by its affinity to the fixed-charged groups of the membrane.

A fraction of the membrane volume is inaccessible for ion transport as it is occupied by the membrane resin and reinforcement. For ions to move across the membrane, a tortuous path inside the membrane is taken. The mobility reduction factor due to the membrane tortuosity can be predicted based on the membrane water volume fraction according to the Mackie and Meares theory [23,24] which explains the ion mobility reduction for Na^+ or K^+ counter-ions (Fig. 4a). For Fuji-12, the K^+ reduction factor based on the conductivity measurement, is significantly higher than the expected reduction factor based on the Mackie and Meares theory. The calculation for this membrane is not corrected for the reinforcement material resistance as we only corrected the membranes with a woven reinforcement. In this regard, the high density of the reinforcement fibers in Fuji-CEM-12 (Fig. 1a) is another significant factor contributing to the membrane resistance.

The membrane tortuosity and reinforcement structure are the main factors reducing the Na^+ and K^+ diffusion coefficients inside the membrane. However, these factors are less significant for the Mg^{2+} and Ca^{2+} mobility reduction factors in most of the membranes, such as the FKS membrane (Fig. 1c). The ratio between the reduction factor of each ion to that of K^+ (Fig. 4b) indicates the additional resistance that each ion faces compared to K^+ ions. Therefore, this ratio is neither affected by the reinforcement material resistance nor the membrane tortuosity. At water volume fractions below 0.6 mL H_2O/mL swollen polymer, the mobilities of Ca^{2+} and Mg^{2+} are reduced by 7–17 times the reduction factor of K^+. The differences between the mobility reduction factors diminish in the membranes containing high water volume fraction (above 0.6 mL H_2O/mL swollen polymer), as exhibited by FKD and FKB.

Generally, the trend of the mobility reduction factors (i.e., $K^+ < Na^+ < Ca^{2+} < Mg^{2+}$, Fig. 4) is similar to the trend of the ion hydrated radius [47], molar hydration volume, and molar hydration energy [48] in aqueous solutions (Table SI-1 and 2). Han et al. [49] studied the water transferred through IEMs in the ion hydration shell where they concluded a significantly higher hydration number for Mg^{2+} (i.e., 15–16) compared to Na^+ (i.e., 6). In nanofiltration membranes, ions with lower hydrated radius exhibited higher permeability through the membrane [50]. In electrodialysis desalination of a single electrolyte solution, the water transport rate (WTR) was higher in case of Cu^{2+} compared to K^+ in four different CEMs for the same applied current density (Fig. 4 in Ref. [51]). Moreover, the higher the membrane water content was, the higher the WTR was.

The counter-ion mobility is reduced to a certain extent based on the membrane properties, e.g., water volume fraction, and the ion properties, e.g., the hydrated radius. The mobility of the different counter-ions can be predicted based on one of the general characteristics of the membrane or based on the mobility of another counter-ion species. We correlated the diffusion coefficients of the different cations (D_i^m [1E-12 m^2/s]) in the membrane to that of Na^+ ($D_{Na^+}^m$ [1E-12 m^2/s]) as follows

$$D_i^m = \alpha_i \cdot \left(D_{Na^+}^m\right)^{\beta_i} \quad \text{Eq. 14}$$

where α and β are ion-specific constants. The subscript, i, refers to any counter-ion in a CEM. The membrane resistance in a NaCl solution is commonly measured for commercial and novel cation-exchange membranes. We fitted the data measured in the present study for the seven commercial CEMs, and calculated two fitting parameters (α and β) for each cation (Fig. 5a, Table 1). When we assume this correlation is not membrane-specific, it can be used to predict the diffusion coefficients of K^+, Mg^{2+}, and Ca^{2+} in any standard CEM based on the measured Na^+

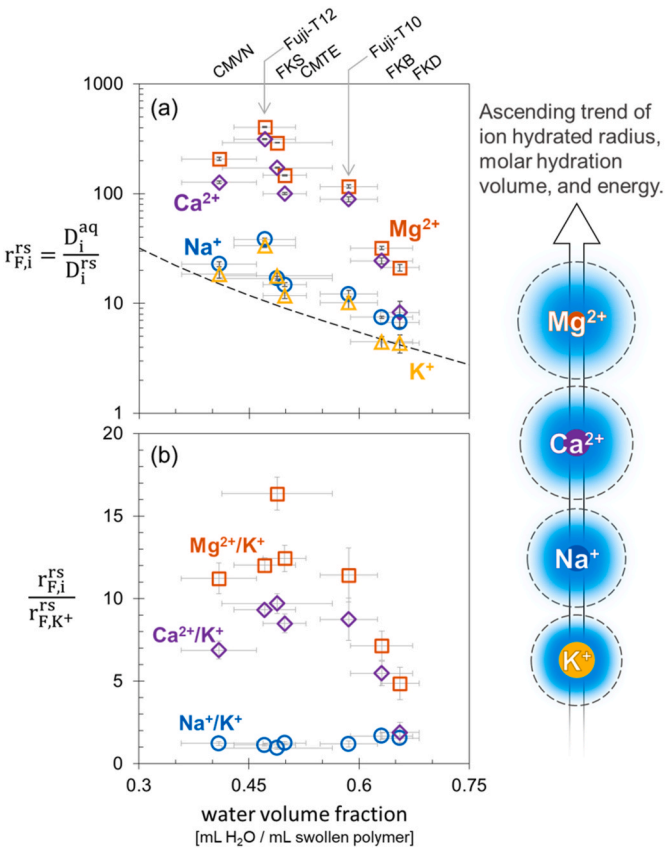

Fig. 4. (a) The mobility reduction factor of counter-ions versus the membrane resin water volume fraction. The data points in each series represent seven different commercial cation-exchange membranes. The data points with the same water volume fraction correspond to the same membrane with different counter-ions. The reduction factor is calculated using the EIS membrane resistance measured at different single electrolyte solutions: 0.5 M NaCl (blue circles), 0.5 M KCl (yellow triangles), 0.25 M $MgCl_2$ (orange squares), and 0.25 M $CaCl_2$ (purple diamonds). The membrane water volume fraction is measured at 0.5 M NaCl via the stacking method as reported in Ref. [23] and the Supporting Info, SI-2. The theoretical tortuosity reduction factor of the ion mobility for an arbitrary membrane water volume fraction is plotted based on Mackie and Meares (dashed line). (b) The ratio between the reduction factor of ion, i, to that of K^+. The horizontal error bars represent the water volume fraction uncertainty which accounts for the measurement uncertainty of the membrane water content (80 % confidence level), wet thickness, and surface area density based on the "addition in quadrature approach" [23]. The vertical error bars reflect the uncertainty in the conductivity measurements. (For interpretation of the references to colour in this figure legend, the reader is referred to the Web version of this article.)

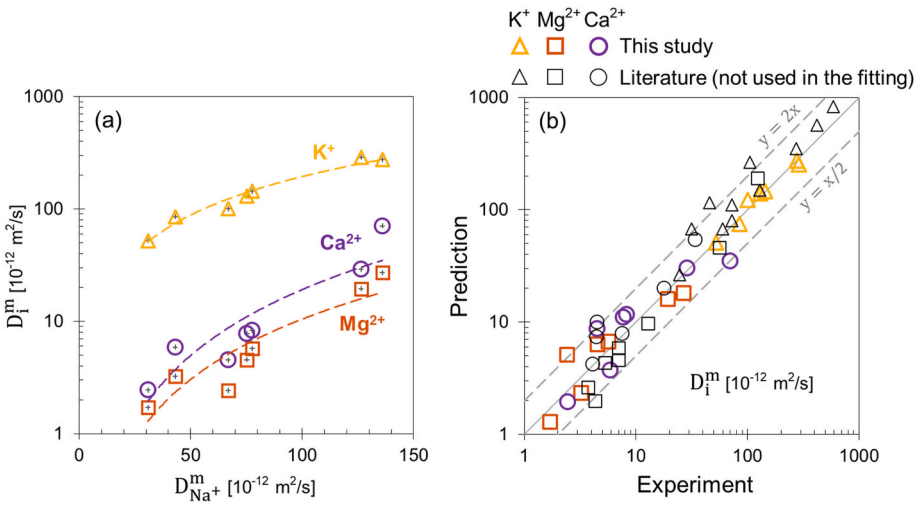

Fig. 5. (a) Experimental diffusion coefficients of K^+ (triangles), Mg^{2+} (squares), and Ca^{2+} (circles) versus the Na^+ diffusion coefficient (x-axis). The data points in each series represent the different commercial membranes investigated in the present study. The error bars reflect the uncertainty in the conductivity measurement. The dashed lines represent the fitting correlations. (b) The predicted diffusion coefficients (y-axis) versus the experimental values (x-axis). The markers in black represent data retrieved from literature that is not used in the fitting. The data are listed in Table SI-6. Dashed grey lines represent the functions y = 2x and y = x/2.

Table 1
The fitting parameters (α and β in Eq. 14) and the coefficient of determination for diffusion coefficient correlation of different counter-ions. The unit of the diffusion coefficients in Eq. 14 is [1E-12 m^2/s].

counter-ion	α_i	β_i	R^2
K^+	1.04	1.14	0.96
Mg^{2+}	2.87E-03	1.78	0.83
Ca^{2+}	2.42E-03	1.95	0.82

diffusion coefficient. We compared the predicted values of the K^+, Mg^{2+}, and Ca^{2+} diffusion coefficients to the experimental values that are available in literature [7,21,25,26,32,39,52–56] for standard CEMs (Fig. 5b). The correlation predictions match the experimental values within an uncertainty factor of 2. In most of the CEMs, the K^+ diffusion coefficient is higher than that of Na^+. However, a few membranes, such as Nafion-117, have a lower mobility of K^+ relative to Na^+. This is explained by the significant decrease in water content of such a membrane when the counter-ions are exchanged from Na^+ to K^+ [53,57].

3.2. Counter-ion mobility at binary mixtures: membrane conductivity

In this section, we discuss the theoretical description of ion mobility within the membrane for a binary mixture. In our recent work, we compared two scenarios for describing the ion mobility inside the membrane for multi-component transport in Donnan dialysis experiments (Figs. SI–7 in Ref. [22]). The first scenario (S1) assumes that counter-ion diffusion coefficients in multi-electrolyte mixtures ($D_i^{m,eff}$) are the same as found in the single electrolyte experiment ($D_i^{m,SE}$)

$$D_i^{m,eff} = D_i^{m,SE} \quad \text{Eq. 15}$$

where "i" refers to the counter-ion species. The second scenario (S2) assigns a single value (a concentration-weighted average, $D_{k_n}^{m,eff}$) to the diffusion coefficient of all the mobile ions in each discretized element (k_n) of the membrane

$$D_{k_n}^{m,eff} = \frac{\sum_i D_i^{m,SE} \cdot C_{i,k_n}^{avg}}{\sum_i C_{i,k_n}^{avg}} \quad \text{Eq. 16}$$

where C_{i,k_n}^{avg} is the average concentration of ion (i) in the discretized element k_n of the membrane. The second scenario (Eq. 16) assumes that the transport of an ion inside the membrane is limited by the mobility of the neighboring ions. Moreover, a third scenario (S3) assigns an average value to all ions based on the equivalent ion concentrations inside the membrane by taking the ion charge into account as follows

$$D_{k_n}^{m,eff} = \frac{\sum_i D_i^{m,SE} \cdot |z_i| \cdot C_{i,k_n}^{avg}}{\sum_i |z_i| \cdot C_{i,k_n}^{avg}} \quad \text{Eq. 17}$$

The ion concentrations inside the membrane are calculated based on Donnan equilibrium conditions and the ion activity coefficients as presented in Ref. [22]. We measured the membrane resistance at a binary mixture of NaCl and $MgCl_2$ where the total Cl^- concentration is 0.5 M and the molar ratio of Na^+:Mg^{2+} is 2:1 (Fig. 6a). The resin conductivity ($\kappa_m^{rs} = 1/\rho_m^{rs}$) is calculated based on the measured membrane resistance (Eq. 8). Furthermore, the three scenarios (Eqs. 15–17) are used to predict the resin conductivity (Eq. 9) using the ion diffusion coefficients in the membrane at single electrolyte solutions. The second scenario (Eq. 16) significantly overestimates the measured resin conductivity (Fig. 6b). Moreover, the scenarios of Eqs. 15 and 17 showed good prediction of the membrane conductivity at binary mixture.

3.3. Counter-ion mobility at binary mixtures: ion fluxes

In this section, we simulate two scenarios (i.e., Eqs. 15 and 17) to predict the counter-ion flux selectivity during electrodialysis experiments involving Na^+/Mg^{2+} binary electrolytes in the under-limiting current regime (Fig. 7). The experimental data were retrieved from literature [16,21,32,39,55,56] for electrodialysis performed with membranes of known characteristics, such as the wet membrane thickness, the ion-exchange capacity, the membrane conductivity for a single electrolyte, as well as the Na^+/Mg^{2+} equilibrium data. The transport model includes three domains: two diffusion and boundary layers and a membrane as described in Ref. [22]. The calculation details are given in the Supporting Info, SI-4. In both scenarios, the total current carried by the cations is set to the experimental value. The Na^+/Mg^{2+} flux selectivity, $S_{Mg^{2+}}^{Na^+}$, is calculated as follows

$$S_{Mg^{2+}}^{Na^+} = \frac{J_{Na^+}/C_{Na^+}}{J_{Mg^{2+}}/C_{Mg^{2+}}} \quad \text{Eq. 18}$$

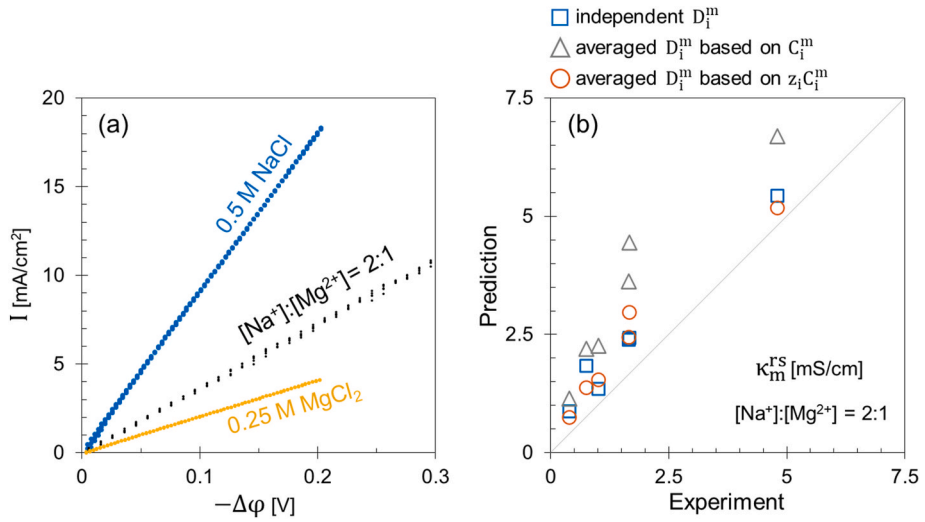

Fig. 6. (a) Current-Voltage curves of CMTE membrane with a single electrolyte of NaCl and $MgCl_2$ as well as a binary mixture of 0.25 M NaCl + 0.125 M $MgCl_2$ (b) prediction of the conductivity of different commercial membranes with a binary mixture of 0.25 M NaCl + 0.125 M $MgCl_2$ versus the experimental value.

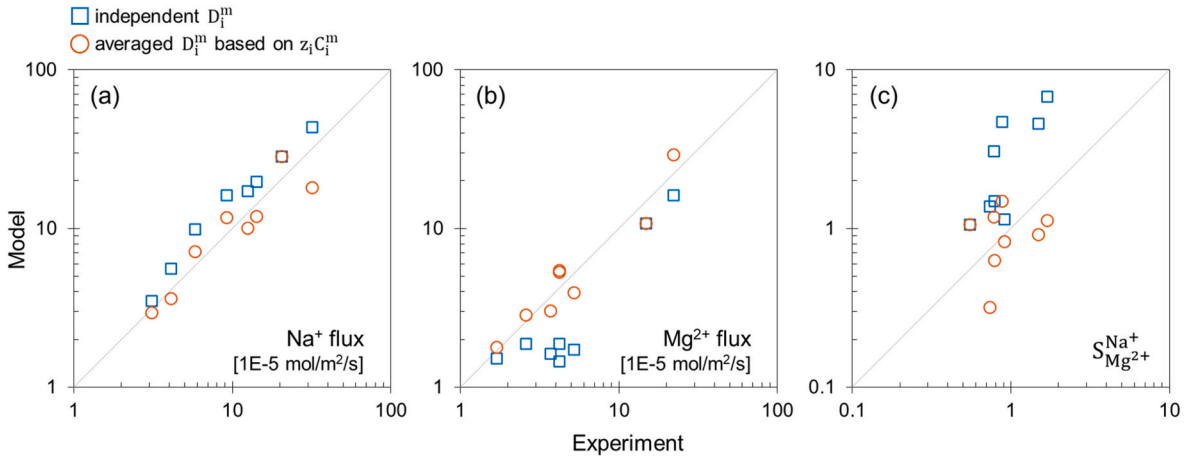

Fig. 7. Comparison between two modeling approaches (y-axis) to simulate electrodialysis of binary mixtures of Na^+ and Mg^{2+} in the under-limiting current regime. The experimental data (x-axis) are retrieved from Refs. [21,32,55]. One model assumes the ion diffusion coefficients inside the membrane to be the same as found in single electrolyte experiments. The other approach assigns an averaged diffusion coefficient to all mobile ions based on the concentration and the charge of the ions inside the membrane element. Each model evaluates (a) the Na^+ flux, (b) the Mg^{2+} flux, and (c) the flux selectivity of Na $^+$ over Mg^{2+}.

where J_i [mol/(m^2·s)] and C_i [mol/m^3] are the flux and the bulk concentration of ion i.

The results of the two scenarios are compared to the experimental values in Fig. 7. The fluxes based on the averaged diffusion coefficient model (S3) are closer to the experimental values than those based on the independent diffusion coefficient model (S1). Using independent diffusion coefficients led to a significant underestimation of the Mg^{2+} flux (Fig. 7b), and consequently overestimating the Na^+/Mg^{2+} selectivity in some experiments (Fig. 7c). For an averaged diffusion coefficient (Eq. 17), the counter-ion selectivity depends on the affinity or activity coefficient of the counter-ions as well as the ion mobility in the diffusion boundary layers. In this regard, the counter-ion flux selectivity can be tuned by using a resin that has a higher affinity for the preferred counter-ion. Moreover, decreasing the diffusion boundary layer thickness improves the fluxes of the faster ion in solution, i.e., the Na^+ ions in case of a Na^+/Mg^{2+} mixture.

In Fig. 8, details of one of the simulated cases are displayed, i.e., the $Na^+/Mg^{2+}/SO_4^{2-}$ electrodialysis experiment across a CMX membrane [21]. Each scenario leads to a different diffusion coefficient profile across the membrane domain (Fig. 8a and b), and consequently, different ion fluxes. In S1, the Mg^{2+} flux is limited by its low mobility inside the CEM. In S3, the averaged diffusion coefficient varies across the CEM domain as the concentrations vary. Compared to S1, the Mg^{2+} flux is higher in S3 leading to a more pronounced depletion of Mg^{2+} in the solution at the DL1/CEM interface (Fig. 8c and d). Therefore, the Mg^{2+} concentration inside the membrane is lower at the DL1 interface relative to the DL2 interface. The Na^+/Mg^{2+} selectivity in S1 and S3 are ca. 1.4 and 0.3, respectively. For this case, the experimental selectivity was measured at 0.7.

Forssell [35] measured the diffusion coefficient of Na^+ ion traces as they diffuse through a CEM containing a specific type of counter-ions. The higher the diffusion coefficient of the surrounding counter-ions was, the higher the diffusion coefficient of the Na^+ tracer ions inside the membrane was. Furthermore, we modeled multi-component ion transport through CEMs in case of Donnan dialysis (Figs. SI–7 in Ref. [22]) as well as electrodialysis (the present study). Using an averaged diffusion coefficient for all cations inside the membrane led to a better match with the experiment compared to using an independent diffusion coefficient for each cationic species. The averaged diffusion coefficient approach (Eq. 17) considers limited space for ion transport. As the ion-exchange membrane has a high fixed-charge concentration, the mobile ions are likely to move from one site to another via

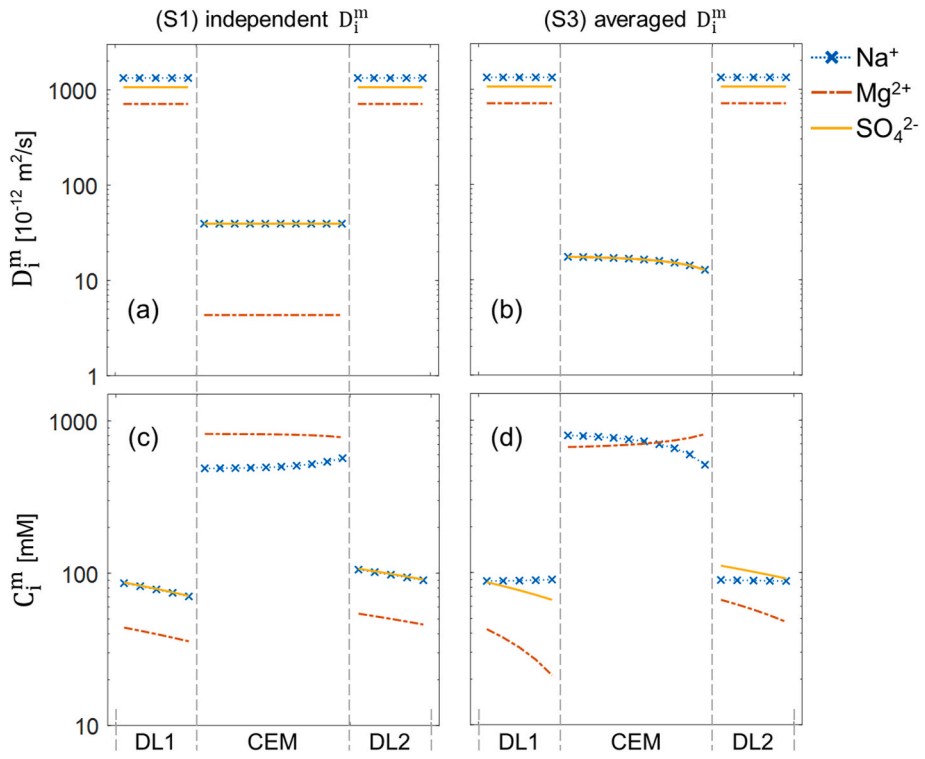

Fig. 8. Calculation results of (a,b) ion diffusion coefficients and (c,d) ion concentration profiles across the diffusion boundary layers (DL1 and DL2) and the cation-exchange membrane (CEM). The plots present the average value of each discretized element. The SO_4^{2-} concentrations inside the membrane are below the plotted range. The left-column plots (a,c) represent the first simulation scenario where the ion diffusion coefficients in the membrane are the same value as determined in the single electrolyte experiments. In the right-column plots (b,d), all ions are assumed to move with an averaged diffusion coefficient based on the charge and concentration of mobile ions in each membrane element. The two scenarios simulate the electrodialysis experiment performed by Luo et al. [21] of Na^+, Mg^{2+}, and SO_4^{2-} across a CMX membrane.

exchanging or taking position of the surrounding counter-ions rather than overtaking the surrounding ions. In this scenario, the diffusion coefficient of an ion depends on its self-diffusion coefficient as well as the self-diffusion coefficients of the surrounding ions. At each position in the membrane, all mobile ions move with a weighted average diffusion coefficient based on the ion concentrations and charges. Since the ion concentrations vary across the membrane, the average diffusion coefficient varies as well (Fig. 8b).

Different strategies can be implemented to separate two cationic species via electrodialysis, e.g., optimizing the stack operating conditions, or tuning the bulk or surface membrane properties. Operating at higher current densities or higher solution flow rates leads to lower ion concentrations in the solution at the CEM interface. Consequently, the transport of the cation whose diffusion coefficient is higher in the aqueous solution is promoted over the slower cation (e.g., K^+ over Na^+, or Na^+ over Mg^{2+}, Fig. 8d). Regarding the membrane bulk properties, CEMs generally have a higher affinity towards Mg^{2+} over Na^+ (Fig. 6 in Ref. [22]). To promote the transport of one cationic species (e.g., Na^+) over another (e.g., Mg^{2+}), the membrane of the least Mg^{2+}/Na^+ equilibrium affinity is preferred and vice versa. Furthermore, using monovalent selective CEMs, e.g. polyelectrolyte multilayer coated CEMs, can significantly enhance the transport selectivity for Na^+ over Mg^{2+} and Ca^{2+} [32,58]. The choice of the CEM type to be coated is critical for the energy consumption of the process. The CEMs of low-to-moderate water volume fractions exhibit about one order of magnitude higher resistances in the presence of Mg^{2+} relative to the Na^+ (Figs. 2b and 4a). Meanwhile, this significant difference in the membrane resistance in the case of Mg^{2+} relative to Na^+ is not effective in separating Na^+ from a Na^+/Mg^{2+} mixture as the Na^+ mobility is limited by the surrounding ions inside the membrane (Fig. 7). Therefore, it is recommended to apply the monovalent selective coating on CEMs that has relatively low resistances. In this regard, the CEM prevents co-ion leakage at low energy cost while the selective coating improves the transport selectivity of Na^+ over Mg^{2+}.

We analyzed two scenarios for the ion mobility during electrodialysis of Na^+/Mg^{2+} binary mixture in the under-limiting current regime. Commercial CEMs have relatively high ionic charge densities (1.6–3.8 mol/L water sorbed, Table 4 in Ref. [23]). In such membranes, the ion hydration shell imposes a spatial constraint on the ion mobility where a cation is hindered from overtaking the surrounding cations. Unlike common cations, the protons can move from one hydronium ion to the neighboring water molecule, i.e., the tunneling transport mechanism [11]. In this regard, the proton mobility is hypothesized to be less or unaffected by the mobility of the surrounding cations inside the CEM. Further experimental work is needed to explore the proton mobility inside the CEMs in ionic mixtures which is relevant for electrodialysis operated in the over-limiting current regime and acid recovery applications.

4. Conclusion

We studied the mobility of different counter-ions Na^+, K^+, Mg^{2+}, and Ca^{2+} inside ion-exchange membranes. In aqueous solutions, the four cations exhibit mobilities in the same order of magnitude. Interestingly, the mobilities of each species are reduced to a different extent in each membrane via different mechanisms. The Na^+ and K^+ mobilities inside the membrane are mainly explained by the membrane tortuosity according to the Mackie and Meares theory. For Mg^{2+} and Ca^{2+}, the mobilities are much more sensitive to the membrane water volume fraction. The Mg^{2+} mobility is further reduced inside the membrane relative to Ca^{2+} followed by Na^+ and K^+, which matches the order of their hydration radii and molar hydration energy in aqueous solutions.

In single electrolyte experiments, the Na^{+} mobility inside the membrane can be an order of magnitude higher than that of Mg^{2+}. In a binary mixture of Na^{+} and Mg^{2+}, the mobility differences attenuate indicating that the mobility of each counter-ion is affected by the mobility of the surrounding ions inside the membrane. In electrodialysis of ionic mixtures, we compared two scenarios for the counter-ion mobilities: either each counter-ion exhibits an independent mobility of each other, or all counter-ions move with an averaged mobility. Using an averaged diffusion coefficient, based on the counter-ion concentrations and ion charges, led to better predictions of the experimental counter-ion fluxes. In this regard, the counter-ion flux selectivity is influenced by the counter-ion partitioning inside the membrane and the ion mobility in the diffusion boundary layers. Moreover, the ratio between the membrane resistance for single electrolytes does not necessarily reflect the actual counter-ion selectivity during electrodialysis of ionic mixtures.

CRediT authorship contribution statement

Alaaeldin A.E. Elozeiri: Writing – original draft, Visualization, Software, Methodology, Investigation, Conceptualization. **Rob G.H. Lammertink:** Writing – original draft, Visualization, Supervision, Methodology, Funding acquisition, Conceptualization. **Shihong Lin:** Writing – original draft, Visualization, Methodology. **Huub H.M. Rijnaarts:** Writing – original draft, Visualization, Supervision, Methodology, Funding acquisition, Conceptualization. **Jouke E. Dykstra:** Writing – original draft, Visualization, Supervision, Methodology, Funding acquisition, Conceptualization.

Declaration of competing interest

The authors declare that they have no known competing financial interests or personal relationships that could have appeared to influence the work reported in this paper.

Acknowledgment

This research was performed within the framework of the research program AquaConnect, funded by the Dutch Research Council (NWO, grant-ID P19-45) and public and private partners of the AquaConnect consortium and coordinated by Wageningen University and Research. The authors thank Wageningen University and Research for the WIMEK Research Fellowship awarded to S.L.

Appendix A. Supplementary data

Supplementary data to this article can be found online at https://doi.org/10.1016/j.memsci.2024.123636.

Data availability

Data will be made available on request.

References

[1] M.A. Alkhadra, et al., Electrochemical methods for water purification, ion separations, and energy conversion, Chem. Rev. 122 (16) (Aug. 2022) 13547–13635, https://doi.org/10.1021/acs.chemrev.1c00396.
[2] L. Janssen, The role of electrochemistry and electrochemical technology in environmental protection, Chem. Eng. J. 85 (2–3) (Jan. 2002) 137–146, https://doi.org/10.1016/S1385-8947(01)00218-2.
[3] A.G. Capodaglio, Fit-for-purpose urban wastewater reuse: analysis of issues and available technologies for sustainable multiple barrier approaches, Crit. Rev. Environ. Sci. Technol. 51 (15) (Aug. 2021) 1619–1666, https://doi.org/10.1080/10643389.2020.1763231.
[4] B.P. Chaplin, The prospect of electrochemical technologies advancing worldwide water treatment, Acc. Chem. Res. 52 (3) (Mar. 2019) 596–604, https://doi.org/10.1021/acs.accounts.8b00611.
[5] H.J. Zwijnenberg, A.A.E. Elozeiri, J. de Grooth, W.G.J. van der Meer, J.A. Wood, Transport characterization and modelling of Donnan dialysis for ammonium recovery from aqueous solutions, J. Memb. Sci. 674 (May 2023) 121496, https://doi.org/10.1016/j.memsci.2023.121496.
[6] Q.-B. Chen, Z.-Y. Ji, J. Liu, Y.-Y. Zhao, S.-Z. Wang, J.-S. Yuan, Development of recovering lithium from brines by selective-electrodialysis: effect of coexisting cations on the migration of lithium, J. Memb. Sci. 548 (Feb. 2018) 408–420, https://doi.org/10.1016/j.memsci.2017.11.040.
[7] D. Ding, L. Yang, J. Wang, A. Yaroshchuk, J.L. Schaefer, M.L. Bruening, Selective transport of trivalent lanthanide in electrodialysis: limitations due to concentration polarization, J. Memb. Sci. 685 (Nov. 2023) 121949, https://doi.org/10.1016/j.memsci.2023.121949.
[8] S.K. Patel, P.M. Biesheuvel, M. Elimelech, Energy consumption of brackish water desalination: identifying the sweet spots for electrodialysis and reverse osmosis, ACS ES&T Eng. 1 (5) (May 2021) 851–864, https://doi.org/10.1021/acsestengg.0c00192.
[9] T. Luo, S. Abdu, M. Wessling, Selectivity of ion exchange membranes: a review, J. Memb. Sci. 555 (Jun. 2018) 429–454, https://doi.org/10.1016/j.memsci.2018.03.051. December 2017.
[10] H. Strathmann, A. Grabowski, G. Eigenberger, Ion-exchange membranes in the chemical process industry, Ind. Eng. Chem. Res. 52 (31) (Aug. 2013) 10364–10379, https://doi.org/10.1021/ie4002102.
[11] H. Strathmann, Ion-Exchange Membrane Separation Processes, first ed., Elsevier Science, Amsterdam, 2004.
[12] J. Zhu, J. Tan, Q. Pan, Z. Liu, Q. Hou, Effects of Mg2+ contamination on the performance of proton exchange membrane fuel cell, Energy 189 (Dec. 2019) 116135, https://doi.org/10.1016/j.energy.2019.116135.
[13] J. Qi, et al., Effect of cationic contaminants on polymer electrolyte fuel cell performance, J. Power Sources 286 (Jul. 2015) 18–24, https://doi.org/10.1016/j.jpowsour.2015.03.142.
[14] D. Huang, B.-Y. Song, Y.-L. He, Q. Ren, S. Yao, Cations diffusion in Nafion117 membrane of microbial fuel cells, Electrochim. Acta 245 (Aug. 2017) 654–663, https://doi.org/10.1016/j.electacta.2017.06.004.
[15] J. Veerman, L. Gómez-Coma, A. Ortiz, I. Ortiz, Resistance of ion exchange membranes in aqueous mixtures of monovalent and divalent ions and the effect on reverse electrodialysis, Membr. 13 (3) (Mar. 2023) 322, https://doi.org/10.3390/membranes13030322.
[16] T. Rijnaarts, E. Huerta, W. van Baak, K. Nijmeijer, Effect of divalent cations on RED performance and cation exchange membrane selection to enhance power densities, Environ. Sci. Technol. 51 (21) (Nov. 2017) 13028–13035, https://doi.org/10.1021/acs.est.7b03858.
[17] A.H. Avci, et al., Effect of Mg2+ ions on energy generation by Reverse Electrodialysis, J. Memb. Sci. 520 (Dec. 2016) 499–506, https://doi.org/10.1016/j.memsci.2016.08.007.
[18] E. Fontananova, et al., Effect of solution concentration and composition on the electrochemical properties of ion exchange membranes for energy conversion, J. Power Sources 340 (Feb. 2017) 282–293, https://doi.org/10.1016/j.jpowsour.2016.11.075.
[19] S. Hidayat, Y.H. Song, J.Y. Park, A comparison of mono- and multi-valent ions as stack feed solutions in microbial reverse-electrodialysis electrolysis cells and their effects on hydrogen generation, Int. Biodeterior. Biodegrad. 113 (Sep. 2016) 28–33, https://doi.org/10.1016/J.IBIOD.2016.03.008.
[20] T.D. Hayes, B.F. Severin, Electrodialysis of highly concentrated brines: effects of calcium, Sep. Purif. Technol. 175 (Mar. 2017) 443–453, https://doi.org/10.1016/J.SEPPUR.2016.10.035.
[21] T. Luo, F. Roghmans, M. Wessling, Ion mobility and partition determine the counter-ion selectivity of ion exchange membranes, J. Memb. Sci. 597 (Mar. 2020) 117645, https://doi.org/10.1016/j.memsci.2019.117645.
[22] A.A.E. Elozeiri, J.E. Dykstra, H.H.M. Rijnaarts, R.G.H. Lammertink, Multi-component ion equilibria and transport in ion-exchange membranes, J. Colloid Interfac. Sci. 673 (Nov. 2024) 971–984, https://doi.org/10.1016/j.jcis.2024.06.025.
[23] A.A.E. Elozeiri, R.G.H. Lammertink, H.H.M. Rijnaarts, J.E. Dykstra, Water content of ion-exchange membranes: measurement technique and influence on the ion mobility, J. Memb. Sci. 698 (Apr. 2024) 122538, https://doi.org/10.1016/j.memsci.2024.122538.
[24] J.S. Mackie, P. Meares, The diffusion of electrolytes in a cation-exchange resin membrane I. Theoretical, Proc. R. Soc. London. Ser. A. Math. Phys. Sci. 232 (1191) (Nov. 1955) 498–509, https://doi.org/10.1098/rspa.1955.0234.
[25] H. Fan, Y. Huang, I.H. Billinge, S.M. Bannon, G.M. Geise, N.Y. Yip, Counterion mobility in ion-exchange membranes: spatial effect and valency-dependent electrostatic interaction, ACS ES&T Eng. 2 (7) (Jul. 2022) 1274–1286, https://doi.org/10.1021/acsestengg.1c00457.
[26] J.C. Díaz, et al., Understanding monovalent cation diffusion in negatively charged membranes and the role of membrane water content, Macromol. 57 (5) (Mar. 2024) 2468–2481, https://doi.org/10.1021/acs.macromol.3c02655.
[27] V.I. Volkov, et al., Mobility of Li+, Na+, Cs+ cations in sulfocation-exchange membranes based on polyethylene and grafted sulfonated polystyrene studied by NMR relaxation, Membr. Membr. Technol. 4 (3) (Jun. 2022) 189–194, https://doi.org/10.1134/S2517751622030076.
[28] V.I. Volkov, et al., Hydration and diffusion of H+, Li+, Na+, Cs+ ions in cation-exchange membranes based on polyethylene- and sulfonated-grafted polystyrene studied by NMR technique and ionic conductivity measurements, Membr. 10 (10) (Oct. 2020) 272, https://doi.org/10.3390/membranes10100272.
[29] L. Dammak, C. Larchet, B. Auclair, J.A. Manzanares, S. Mafé, The influence of the salt concentration and the diffusion boundary layers on the bi-ionic potential,

J. Memb. Sci. 119 (1) (Oct. 1996) 81–90, https://doi.org/10.1016/0376-7388(96)00100-7.
[30] J. Kamcev, D.R. Paul, G.S. Manning, B.D. Freeman, Ion diffusion coefficients in ion exchange membranes: significance of counterion condensation, Macromol. 51 (15) (Aug. 2018) 5519–5529, https://doi.org/10.1021/acs.macromol.8b00645.
[31] Y. Huang, H. Fan, N.Y. Yip, Mobility of condensed counterions in ion-exchange membranes: application of screening length scaling relationship in highly charged environments, Environ. Sci. Technol. 58 (1) (Jan. 2024) 836–846, https://doi.org/10.1021/acs.est.3c06068.
[32] T. Rijnaarts, D.M. Reurink, F. Radmanesh, W.M. de Vos, K. Nijmeijer, Layer-by-layer coatings on ion exchange membranes: effect of multilayer charge and hydration on monovalent ion selectivities, J. Memb. Sci. 570–571 (October 2018) (Jan. 2019) 513–521, https://doi.org/10.1016/j.memsci.2018.10.074.
[33] R.H. Stokes, L.A. Woolf, R. Mills, Tracer diffusion of iodide ion in aqueous alkali chloride solutions at 25, J. Phys. Chem. 61 (12) (Dec. 1957) 1634–1636, https://doi.org/10.1021/j150558a016.
[34] T. Okada, H. Satou, M. Okuno, M. Yuasa, Ion and water transport characteristics of perfluorosulfonated ionomer membranes with H + and alkali metal cations, J. Phys. Chem. B 106 (6) (Feb. 2002) 1267–1273, https://doi.org/10.1021/jp013195l.
[35] P. Forssell, I. Grenthe, S. Hietanen, F. Salvatore, L. Niinistö, Determination of the tracer diffusion coefficient in a cation exchange membrane, Acta Chem. Scand. 41a (1987) 269–273, https://doi.org/10.3891/acta.chem.scand.41a-0269.
[36] S.A. Mareev, D.Y. Butylskii, N.D. Pismenskaya, C. Larchet, L. Dammak, V. V. Nikonenko, Geometric heterogeneity of homogeneous ion-exchange Neosepta membranes, J. Memb. Sci. 563 (Oct. 2018) 768–776, https://doi.org/10.1016/j.memsci.2018.06.018.
[37] W. Zhang, J. Ma, P. Wang, Z. Wang, F. Shi, H. Liu, Investigations on the interfacial capacitance and the diffusion boundary layer thickness of ion exchange membrane using electrochemical impedance spectroscopy, J. Memb. Sci. 502 (Mar. 2016) 37–47, https://doi.org/10.1016/j.memsci.2015.12.007.
[38] E. Stránská, D. Neděla, Reinforcing fabrics as the mechanical support of ion exchange membranes, J. Ind. Text. 48 (2) (Aug. 2018) 432–447, https://doi.org/10.1177/1528083717732075.
[39] V. Sarapulova, et al., Transport characteristics of Fujifilm ion-exchange membranes as compared to homogeneous membranes AMX and CMX and to heterogeneous membranes MK-40 and MA-41, Membr. 9 (7) (Jul. 2019) 84, https://doi.org/10.3390/membranes9070084.
[40] P. Długołęcki, B. Anet, S.J. Metz, K. Nijmeijer, M. Wessling, Transport limitations in ion exchange membranes at low salt concentrations, J. Memb. Sci. 346 (1) (Jan. 2010) 163–171, https://doi.org/10.1016/j.memsci.2009.09.033.
[41] P.M. Biesheuvel, J.E. Dykstra, Physics of Electrochemical Processes, 2020.
[42] F.G. Donnan, The theory of membrane equilibria, Chem. Rev. 1 (1) (Apr. 1924) 73–90, https://doi.org/10.1021/cr60001a003.
[43] P. Długołęcki, P. Ogonowski, S.J. Metz, M. Saakes, K. Nijmeijer, M. Wessling, On the resistances of membrane, diffusion boundary layer and double layer in ion exchange membrane transport, J. Memb. Sci. 349 (1–2) (Mar. 2010) 369–379, https://doi.org/10.1016/j.memsci.2009.11.069.
[44] Y. Huang, H. Fan, N.Y. Yip, Influence of electrolyte on concentration-induced conductivity-permselectivity tradeoff of ion-exchange membranes, J. Memb. Sci. 668 (Feb. 2023) 121184, https://doi.org/10.1016/j.memsci.2022.121184.
[45] S. Zhu, R.S. Kingsbury, D.F. Call, O. Coronell, Impact of solution composition on the resistance of ion exchange membranes, J. Memb. Sci. 554 (May 2018) 39–47, https://doi.org/10.1016/j.memsci.2018.02.050.
[46] F.G. Helfferich, *Ion Exchange*, No. 3, McGraw-Hill, 1962.
[47] E.R. Nightingale, Phenomenological theory of ion solvation. Effective radii of hydrated ions, J. Phys. Chem. 63 (9) (Sep. 1959) 1381–1387, https://doi.org/10.1021/j150579a011.
[48] Y. Marcus, Thermodynamics of solvation of ions. Part 5.—gibbs free energy of hydration at 298.15 K, J. Chem. Soc., Faraday Trans. 87 (18) (Jan. 1991) 2995–2999, https://doi.org/10.1039/FT9918702995.
[49] L. Han, S. Galier, H. Roux-de Balmann, Ion hydration number and electro-osmosis during electrodialysis of mixed salt solution, Desalination 373 (Oct. 2015) 38–46, https://doi.org/10.1016/j.desal.2015.06.023.
[50] B. Tansel, et al., Significance of hydrated radius and hydration shells on ionic permeability during nanofiltration in dead end and cross flow modes, Sep. Purif. Technol. 51 (1) (Aug. 2006) 40–47, https://doi.org/10.1016/j.seppur.2005.12.020.
[51] C. Jiang, Q. Wang, Y. Li, Y. Wang, T. Xu, Water electro-transport with hydrated cations in electrodialysis, Desalination 365 (Jun. 2015) 204–212, https://doi.org/10.1016/j.desal.2015.03.007.
[52] G. Pourcelly, P. Sistat, A. Chapotot, C. Gavach, V. Nikonenko, Self diffusion and conductivity in NafionR membranes in contact with NaCl+CaCl2 solutions, J. Memb. Sci. 110 (1) (Feb. 1996) 69–78, https://doi.org/10.1016/0376-7388(95)00232-4.
[53] I.A. Stenina, P. Sistat, A.I. Rebrov, G. Pourcelly, A.B. Yaroslavtsev, Ion mobility in Nafion-117 membranes, Desalination 170 (1) (Oct. 2004) 49–57, https://doi.org/10.1016/j.desal.2004.02.092.
[54] V.V. Sarapulova, V.D. Titorova, V.V. Nikonenko, N.D. Pismenskaya, Transport characteristics of homogeneous and heterogeneous ion-exchange membranes in sodium chloride, calcium chloride, and sodium sulfate solutions, Membr. Membr. Technol. 1 (3) (May 2019) 168–182, https://doi.org/10.1134/S2517751619030041.
[55] L. Wu, T. Luo, X. Yang, H. Zhao, X. Wang, Z. Zhang, Impact of the Donnan electrolytes on selectivity of cation exchange membranes evaluated via the ionic membrane conductivity, Sep. Purif. Technol. 316 (Jul. 2023) 123816, https://doi.org/10.1016/j.seppur.2023.123816.
[56] C. Espinoza, D. Kitto, J. Kamcev, Counter-ion conductivity and selectivity trade-off for commercial ion-exchange membranes at high salinities, ACS Appl. Polym. Mater. (Nov. 2023), https://doi.org/10.1021/acsapm.3c02102.
[57] G. Xie, T. Okada, The state of water in nafion 117 of various cation forms, Denki Kagaku Oyobi Kogyo Butsuri Kagaku 64 (6) (Jun. 1996) 718–726, https://doi.org/10.5796/kogyobutsurikagaku.64.718.
[58] S. Abdu, M.-C. Martí-Calatayud, J.E. Wong, M. García-Gabaldón, M. Wessling, Layer-by-Layer modification of cation exchange membranes controls ion selectivity and water splitting, ACS Appl. Mater. Interfac. 6 (3) (Feb. 2014) 1843–1854, https://doi.org/10.1021/am4048317.